Modeling Outdoor Service Lifetime Prediction of PV Modules: Effects of Combined Climatic Stressors on PV Module Power Degradation

Ismail Kaaya, Michael Koehl, Amantin Panos Mehilli, Sidrach de Cardona Mariano, and Karl Anders Weiss

***Abstract*—Photovoltaic modules are exposed to a variety of climatic loads during outdoor operation. Over time, these loads trigger a number of degradation modes within the modules leading to performance loss. This paper quantifies the impact of combined climatic loads on the module's maximum power output using a mathematical approach. Three degradation precursor reactions, namely, hydrolysis, photodegradation, and thermomechanical degradation, are assumed to be necessary for service lifetime prediction. For each reaction, an empirical kinetics model is proposed and validated with indoor test measurements. A generalized model to quantify the effects of combined climatic loads is proposed. The generalized model is calibrated and validated using outdoor test measurements. The model is then applied to predict the annual degradation rates and a 20% performance loss of three identical monocrystalline modules installed in three benchmarking climates: maritime (Gran Canaria, Spain), arid (Negev, Israel), and alpine (Zugspitze, Germany) using real monitored meteorological data. A degradation of 0.74%/year corresponding to 21.4 years operation time was predicted as the highest for an arid environment, compared with 0.50%/year and 0.3%/year degradation for maritime and alpine environments, respectively. The proposed models will find applications in outdoor predictions as well as in the combined stress accelerated tests to develop test designs.**

***Index Terms*—Climatic zones and service lifetime prediction, degradation model, degradation modes, photovoltaic (PV) module.**

I. Introduction

THE search for a combined stress model for photovoltaic (PV) module lifetime prediction dates back to the 1970s, for example, Gaines *et al*. [1] proposed a quantitative model for accelerated testing using multiple environmental stresses, which was used to develop the test design. Recently, Subramaniyan *et al*. [2] have proposed a model to link the module degradation path and environmental variables. According to our previous publication [3], the current state-of-the-art degradation models available for PV modules and systems were reviewed. Among the key observations was that most of the degradation models are developed for specific degradation modes using controlled test conditions and are validated based on indoor measurements from accelerated tests. Since a PV module in outdoor operation experiences numerous climatic loads, which, in turn, might lead to different degradation modes, combined stress models are a prerequisite to estimate PV module degradation.

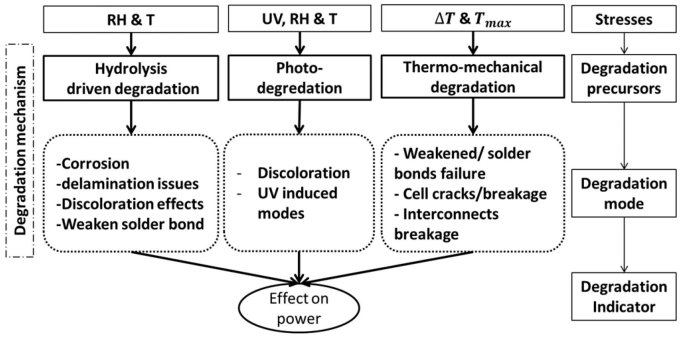

Fig. 1. Schematic diagram of the modeling hypotheses.

The main motivation of this paper is to bridge the gap toward service lifetime prediction of PV modules in outdoor operation. A combined stress model is proposed based on the physics of failure. The approach deployed in this paper is based on analyzing and modeling degradation modes under various climatic stresses. The input stresses are assumed to be responsible for triggering a specific reaction that might induce specific degradation modes (see Fig. 1). The effect of the applied stresses has been evaluated with experimental data using accelerated ageing tests. We assume that it is a crucial step to first evaluate the effects of different stresses in controlled conditions using accelerated tests. This is needed to correlate the power degradation to specific degradation modes using different characterization methods. It also helps to understand the physics of failure of the different degradation modes.

Three main aspects need to be considered for a modeling approach applicable for PV service lifetime prediction.

1) *Impact of PV material variations:* New materials are proposed frequently to improve PV performance.

Manuscript received January 31, 2019; revised March 21, 2019 and April 26, 2019; accepted May 3, 2019. Date of publication May 22, 2019; date of current version June 19, 2019. This work was supported in the framework of the European Union's Horizon 2020 Marie Skłodowska-Curie Actions Program (SOLAR-TRAIN project) under Grant 721452. *(Corresponding author: Ismail Kaaya.)*

I. Kaaya is with the Fraunhofer Institute of Solar Energy, 79110 Freiburg, Germany, and also with the University of Malaga, 29016 Malaga, Spain (e-mail: ismail.kaaya@ise.fraunhofer.de).

M. Koehl, A. P. Mehilli, and K. A. Weiss are with the Fraunhofer Institute of Solar Energy, 79110 Freiburg, Germany (e-mail: Michael.koehl@ise.fraunhofer.de; amantin-Panos.mehilli@ise.fraunhofer.de; karl-anders.weiss@ise.fraunhofer.de).

S. de Cardona Mariano is with the University of Malaga, 29016 Malaga, Spain (e-mail: msidrach@ctima.uma.es).

Color versions of one or more of the figures in this paper are available online at http://ieeexplore.ieee.org.

Digital Object Identifier 10.1109/JPHOTOV.2019.2916197

2) *Different operating climatic conditions:* PV modules operate in different climates, for example, in arid, maritime, tropical climates.
3) Different PV technologies, for example, crystalline silicon (c-Si), thin films, and different module designs like bifacial, glass–glass, or glass–backsheet.

All these factors might lead to different degradation modes, rates, and performance degradation. To our knowledge, it is a rather complex challenge to have a single model taking into account all the above aspects. In this paper, a simplified approach is proposed, as a first approximation to take into account some of the above aspects in a single model.

II. Power Degradation Function and Degradation Rate Models

The fact that the module is exposed to several stress factors at the same time, and that outdoor conditions have a stochastic nature, makes it difficult to model outdoor conditions. A model that includes all the above dependences requires a huge number of unknown coefficients to be evaluated. Some of the required coefficients might require experimental procedures to be evaluated, making it time consuming and expensive.

One way to overcome these obstacles is to use an approach that minimizes the number of coefficients to be evaluated. Assumptions should be made based on the dominating loads, processes, impacts, or mechanisms for degradation evaluation. Constant or average quantities might be used to compute the average rates, in order to overcome the stochastic behavior of input parameters. Using accelerated tests to quantify the impact of applied loads on power degradation and to evaluate the sensitivity of model parameters for varying controlled test conditions helps to start with modeling before investigating outdoor conditions. This also helps to relate the performance losses to specific degradation modes. However, one of the major pitfalls of accelerated testing is that it may focus on one degradation mode while masking others. The masked degradation modes could be the first to show up or dominate in the field under different operating conditions [4]. Therefore, the underlying physics and chemistry related to the degradation must be known to avoid these obstacles. The assumptions and hypotheses used in this paper are based on the prior knowledge and studies [5]–[9], [11]–[15], which deal with the underlying physical and or chemical degradation kinetics. Fig. 1 summarizes the hypothesized degradation mechanisms that are known to be induced by the applied loads.

The models should be calibrated using nonextreme test conditions in order to obtain a good correlation of the indoor accelerated conditions to outdoor conditions. As already mentioned, very extreme conditions might generate new degradation modes that might never happen outdoors [4]; using these conditions for calibration of the model might result in high uncertainties. Moreover, some of the degradation patterns observed in accelerated tests are unlikely to occur in natural aging leading to misinterpretations. For example, during an extended damp heat (DH) test, three phases of power degradation were described by Koehl *et al*. [15] as induction, degradation, and saturation phases. One way to use such a degradation pattern for outdoor ageing would be to use the induction and the onset of the degradation phase as it might be a good representation of natural degradation.

A. Module Output Power Degradation Function

Since the module power at the maximum power point (P_{MPP}) is a quantity commonly used by manufacturers to set warranties, it has been selected for use as a degradation indicator in this paper. Hence, in this context, degradation is defined as the gradual deterioration in the module P_{MPP} over time. The effects of applied climatic stresses are then quantified by how much they lead to a reduction in the initial power over time. The module output power as a function of time is proposed as

$$\frac{P_{\mathrm{MPP}}(t)}{P_{\mathrm{MPP}}(0)} = 1 - \exp\left(-\left(\frac{B}{k_i t}\right)^{\mu}\right) \tag{1}$$

where $P_{\mathrm{MPP}}(t)$ and $P_{\mathrm{MPP}}(0)$ are the module output power at time t and the initial output power, respectively. B is the power susceptibility, which is assumed to be a material property, μ is the shape parameter, and k_i is the degradation rate constant of degradation process i.

B. Degradation Rate Models for Controlled Indoor Conditions

Empirical kinetics models to evaluate the degradation rate constant k_i are proposed depending on the applied stresses as presented in the following general reaction equation:

$$\mathrm{Stress}\ A + \mathrm{Stress}\ B + \ldots \mathrm{Stress}\ N \rightarrow \mathrm{Degradation\ precursor}. \tag{2}$$

In this paper, three main degradation precursor reactions are assumed to be hydrolysis, photodegradation, and thermomechanical degradation. Depending on the applied stresses, a reaction constant is evaluated to quantify the impact of the applied stresses on power degradation over a specified time period.

1) Hydrolysis-Driven Degradation Due to Temperature and Relative Humidity:

$$k_H = A_H . rh_{\mathrm{eff}}^{n} . \exp\left(-\frac{E_H}{k_B . T_m}\right) \tag{3}$$

where k_H is the rate constant, k_B is the Boltzmann constant (8.62×10^{-5}), T_m is the module temperature (Kelvin), A_H is the pre-exponential constant, $rh_{\mathrm{eff}}(\%)$ is the effective module relative humidity (RH) proposed by Koehl *et al.* [16], and n is a model parameter that indicates the impact of RH on power degradation. In this context, E_H is defined as the activation energy for power degradation. Equation (3) is the commonly used Peck's model, which evaluates the degradation impact due to RH and temperature [17]. The Peck's model was selected based on the study of our previous article [3], since the model showed the best performance in DH result calibration.

2) Photodegradation Due to UV Dose, Temperature, and Relative Humidity:

$$k_P = A_P . (\mathrm{UV_{dose}})^{X} . (1 + rh_{\mathrm{eff}}^{n}) . \exp\left(-\frac{E_P}{k_B . T_m}\right) \tag{4}$$

where k_P is the rate constant, $\mathrm{UV_{dose}}$ is the integral UV dose ($\mathrm{kW/m^2}$), E_P is the activation energy for power degradation due

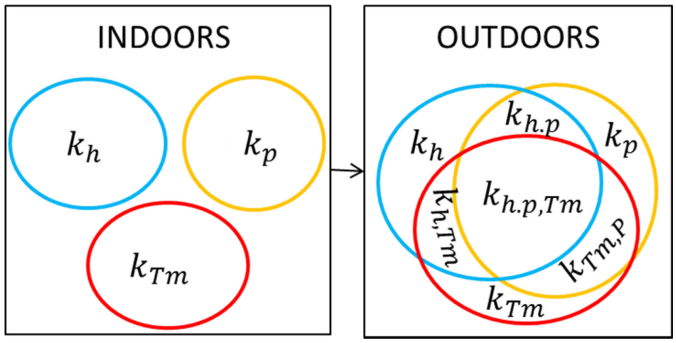

Fig. 2. Schematic diagram showing rates in controlled indoor conditions and the synergistic nature of outdoor conditions.

to photoreaction, and X is a model parameter that indicates the impact of UV dose on power degradation.

3) Thermomechanical Degradation Due to Temperature Cycles: The most commonly used model for thermal cycling (TC) is the Coffin–Manson relationship. According to Escobar and Meeker [17], the effect of temperature cycling can depend largely on the maximum temperature T_U. The cycle-to-failure distribution for temperature cycling can also depend on the cycling rate (e.g., due to heat buildup). Therefore, a modified form of the Coffin–Manson relationship including this effect is

$$k_{Tm} = A_{Tm}.(\Delta T)^{\theta}.C_N.\exp\left(-\frac{E_{Tm}}{k_B.T_U}\right) \tag{5}$$

where $\Delta T = (T_U - T_L)$ is the temperature difference (Kelvin), C_N is the cycling rate, T_U and T_L are the module upper and lower limit temperatures, and E_{Tm} is the activation energy of power degradation.

C. Degradation Rate Model for Outdoor Conditions

The transition from indoor degradation rate evaluation to outdoor is a challenging task due to not yet knowing enough how different stresses, degradation processes, and the induced degradation interact.

The underlying assumption deployed in this paper is that some degradation processes might lead to specific degradation modes independent of the others, and that some might have a synergistic nature (see Fig. 2), which results in a variety of degradation modes. Hence, this assumption allows us to evaluate the total degradation rate as the sum of both independent and dependent processes. The mathematical form of the total rate is expressed as

$$k_T = A_N.(1+k_h)(1+k_p)(1+k_{Tm}) - 1 \tag{6}$$

$$k_T = A_N.\prod_{i=1}^{n}(1+k_i) - 1 \tag{7}$$

where k_T $(\%/\text{year})$ is the total degradation rate $(\%/\text{year})$, k_i is the ith rate constant, and n is the total number of degradation processes. A_N is the normalization constant of the physical quantities; in this case, it takes the units $(\text{year}^{-2}/\%)$.

Using (1) and (7) and defining failure time (t_f) as a 20% loss in maximum power output (common manufacturer's warranty), the failure time can be calculated using the following relation:

$$t_f = \frac{B}{k_T \times [|\log(0.2)|]^{\frac{1}{\mu}}}. \tag{8}$$

TABLE I
EXPERIMENTAL (EXP) CONDITIONS FOR DH COMBINED UV/DH AND TC TESTS

Exp	Models calibration test Conditions	Models Validation test conditions
DH	75°C/85%RH (6500 hours)	85°C/85%RH (6500 hours)
UV/DH	180W/m^2/65°C/55% RH (4000 hours)	180W/m^2/85°C/55% RH (4000 hours)
TC	-40°C/40°C (3500 cycles)	-40°C/85°C (1200 cycles)

III. MODEL CALIBRATION

Two basic approaches were applied for the calibration of the different degradation rate models: 1) optimization of model performances; and 2) through prior knowledge from previous studies. Optimization of model performance, which compares measured and simulated data, was applied with the help of a built-in nonlinear least-squares solver in the *GNU Octave* software. Prior knowledge, with the aid of sensitivity analysis, was used as a baseline to select the initial fitting guesses and also as a confirmation that the extracted values are in meaningful range.

A. Experimental Indoor

Distributed DH, TC, and combined DH-UV stress tests were carried out at different test conditions under the framework of the SOPHIA project at different test laboratories. Table I shows the different test conditions used in this paper for model calibration and validation. The studied modules are from the same manufacturer. They are P-type homojunction c-Si with thermoplastic encapsulant material and without an aluminium layer as additional moisture barrier.

B. Experimental Outdoor

Three identical monocrystalline silicon (mc-Si) modules are under monitoring in three climatic zones: maritime (in Gran Canaria, Spain), arid (in Negev, Israel), and alpine (in UFS Zugspitze, Germany). In Gran Canaria, the tilt angle is 23°, and the azimuth angle 169° for the PV module. In Negev, the tilt angle is 31°, and the azimuth angle 180° for PV modules. The module in Gran Canaria has been exposed for over seven years, and the ones in Negev and Zugspitze have been exposed over five years outdoors.

Apart from the performance measurements, the modules temperatures are also recorded every 10 min. The sensors for measuring module temperatures are located under one of the central cells. They are Pt100 sensors, which are attached from the back using adhesive aluminum tapes. Other meteorological data such as RH, global irradiation, UV irradiance, and wind speed are

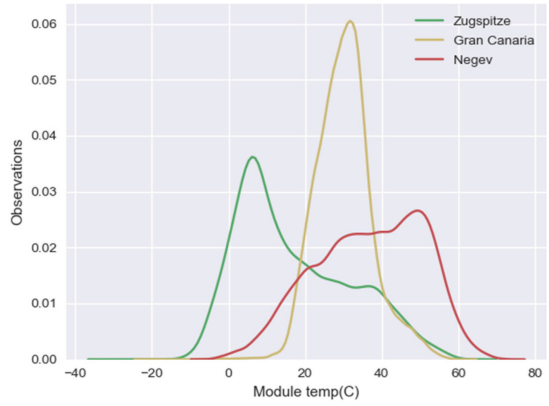

Fig. 3. Distribution of module temperature in the three climatic zones.

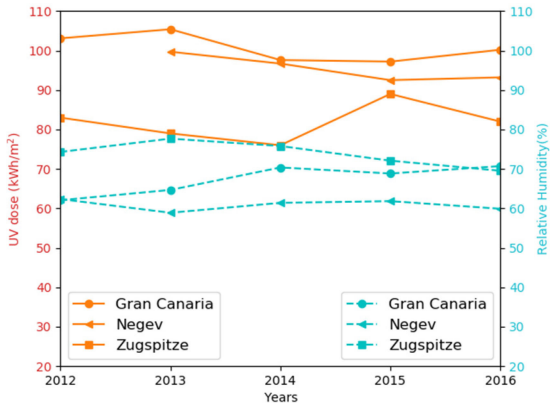

Fig. 4. Total UV dose and average annual RH for the three zones measured for five years.

TABLE II
SUMMARY OF FIVE YEARS AVERAGE CLIMATIC INPUTS USED IN SIMULATION

Location	RH (%)	T_m (°C)	UV dose (kWh/m^2)	T_U (°C)	T_L (°C)
Negev	61.0	36.8	87.7	56.7	12.5
Canaria	68.0	30.6	101.0	43.6	19.6
Zugspitze	74.0	18.7	81.0	44.7	-2.30

also under monitoring in all the three zones with a 1-min resolution. The annual averages of UV dose and RH are as shown in Fig. 4.

Five years of measured datasets were used to evaluate the averages (see Table II), to ensure that the values used in degradation prediction correspond to what a module will experience during its lifetime. The mean value of the module minimum and maximum temperature has been computed considering upper and lower temperature bins as in Fig. 5.

IV. Results and Discussion

A. Model Properties

It is rather complex to develop a generalized model that covers all these requirements for taking into account innovations in materials and designs. Moreover, validation of such a model

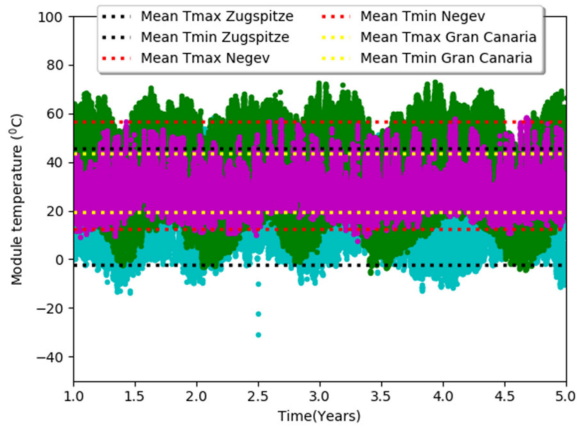

Fig. 5. Ten minutes values of module temperature for five years. The dotted lines show the mean maximum and minimum temperatures.

requires a huge amount of data and experimental campaigns. Although the model parameters are technology or module specific, the formulations presented in this paper are flexible and can be adapted for application in other modules designs and technologies.

On the one hand, extracting model parameters for each evaluated PV module type makes degradation prediction more complex and rather expensive and time consuming. In this case, a model parameter B in (1), the so-called power susceptibility, is introduced. It could allow simulating a percentage increase in performance due to an improvement in materials of different PV modules when other model parameters are kept constant.

On the other hand, we assume that the power degradation shapes could be linked to module technologies or module design. For example, a faster degradation at early stages of exposure and followed by stabilization is commonly observed in thin-film modules [18]. The other speculation is made on the module design, for example, glass–glass modules have less moisture pathways and moisture ingress compared with glass–backsheet modules. This means that moisture-induced degradation modes are slower at the earlier stages of the module lifetime. However, as the breathable pathways and drying are also limited, the moisture will accumulate over the years, leading to a dramatic increase in the degradation rate. For this case, one could expect a degradation shape like that in Fig. 6 when $\mu = 0.96$.

The proposed power degradation function includes a shape parameter μ, making it possible to optimize all the possible degradation shapes. Fig. 6 shows degradation shapes optimization by changing the value of μ.

Moreover, it is very crucial to optimize the power degradation shapes, since they are linked to energy yield evaluation as the yield corresponds to the integral of power with respect to operation time, hence the area under the curves in Fig. 6.

B. Sensitivity Analysis of Input Loads

A sensitivity analysis of climatic input loads of temperature, RH, and UV dose on the failure time was carried out. Temperature (T), RH, and UV dose bins between (15–55 °C), (40–100%), and (80–100 kW/h/m^2), respectively, were used to generate 500

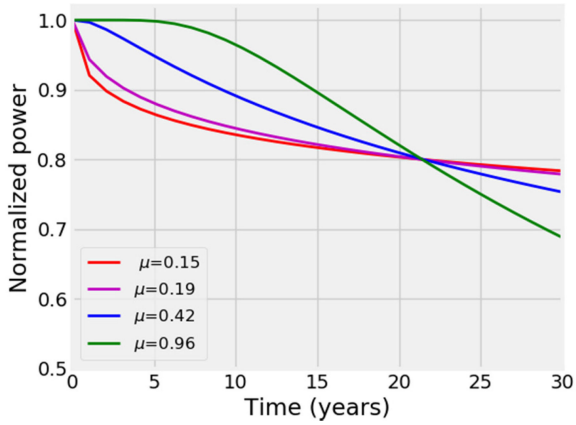

Fig. 6. Optimization of power degradation shapes by altering the shape parameter μ.

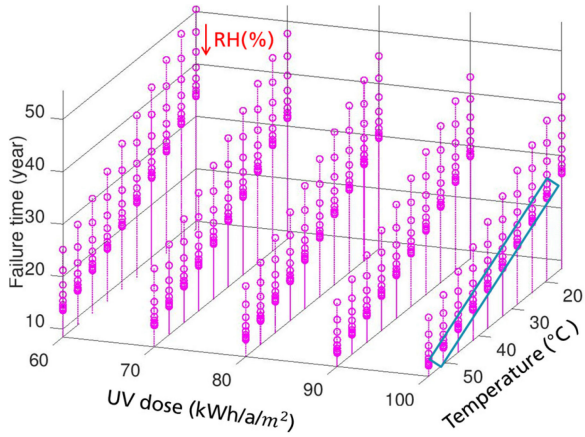

Fig. 7. Sensitivity analysis of T, UV, and RH. The arrow indicates increasing RH represented by the dots.

combinations of *T*, RH, and UV. The variation of failure time to each combination set is shown in Fig. 7.

According to this analysis, the model is more sensitive to temperature as compared with RH and UV dose; this can be explained by the Arrhenius temperature dependence in the rate models. Moreover, during the sensitivity analysis, a threshold of RH (highlighted in blue) was observed. This was linked to the Peck's model for hydrolysis. Simulations using the peck's model only to evaluate the failure time confirmed this tendency at humidity levels above 80%. The model is still applicable, since these conditions are not usually the case outdoors, and in this paper, the varying input load was temperature for indoor conditions.

C. Model Validation

As for any predictive model, the crucial part is to validate the model. There are several ways of model validation. In this paper, the approach used is verification with real experimental measurements. Fig. 8 shows the steps used for validation of the models.

1) Model Validation With Indoor Datasets: The proposed models (3)–(5) were calibrated using indoor experimental data

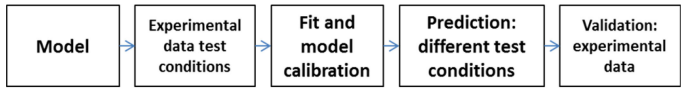

Fig. 8. Schematic diagram of models' calibration and validation procedure using for both indoor and outdoor datasets.

TABLE III
EXTRACTED MODEL PARAMETERS FOR INDOOR MODULES AND THE PERCENTAGE DEVIATION (DEV) FROM THE FITTED DATA

Model	A_i	n	X, θ	$E_a (eV)$	dev
Hydrolysis (3)	6.11e4	1.90	-	0.91	0.5%
Photo-degradation (4)	1.20e-3	1.80	0.63	0.43	0.2%
Thermo-mechanical (5)	9.10e-5	-	2.24	0.40	1.6%

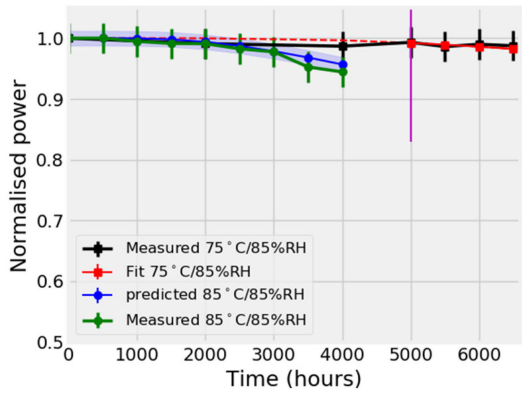

Fig. 9. Hydrolysis model (3) calibration and validation. The blue patch is the 95% confidence interval of prediction; the violet line represents the optimized data points.

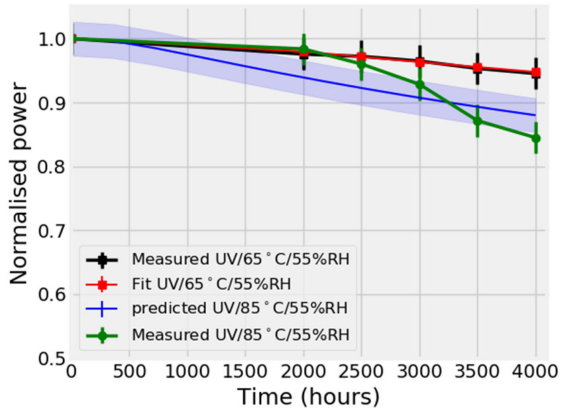

Fig. 10. Photodegradation model (4) calibration and validation. The blue patch is the 95% confidence interval of prediction.

for specific test conditions. The extracted rate models parameters are presented in Table III. The parameter B in (1) was normalized to one, and the extracted shape parameter μ was 0.7 for Fig. 9 and 0.4 for Figs. 10 and 11.

It should be noted that the extracted parameters are valid only for a particular module type. The parameters have to be evaluated for each different module separately. The models were then

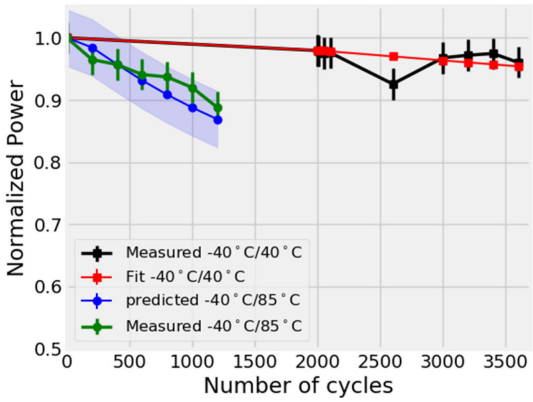

Fig. 11. Thermomechanical model (5) calibration and validation. The blue patch is the 95% confidence interval of prediction.

applied to predict the degradation when the test conditions are varied. The model predictions are compared with experimental outcomes for validation.

Fig. 9 shows calibration and validation results for the hydrolysis model (3). In black is the measured power for DH 75 °C/85RH; red is the respective model fit with a violet line at 5000 h representing the optimized data points. The blue line is the predicted power at DH 85 °C/85RH, the light blue patch is the 95% prediction confidence interval; green represents the measured power at DH 85°C/85RH, used for model validation. The vertical lines on measured data points indicate a 2.5% measurement uncertainty. The color usage and explanation above are consistent with Figs. 10 and 11 for photodegradation (4) and thermomechanical (5) models using respective datasets. For all the models, the predictions are satisfactory and are within a 95% confidence interval. The observable variations could be linked with the measurement uncertainties.

To correlate the uncertainties in model calibration with the predictions, the percentage mean square error of prediction (MSEP) [19] was evaluated as

$$\mathrm{MSEP} = 100 \times \left[V\left[P_p\right] + \left(\mu_{P_p} - \mu_{P_m}\right)^2\right] \tag{9}$$

where P_p and P_m are the predicted and measured power, respectively, V is the variance of the predicted power, and μ_{P_p} and μ_{P_m} are the mean of predicted and measured powers, respectively.

A 0.5% deviation led to 0.025% MSEP for the hydrolysis model, 1.65% deviation resulted into 0.216% MSEP for the thermomechanical model, and 0.19% deviation led to 0.168% MSEP for the photodegradation model. Although there is a correlation of the uncertainties due to model calibration as it is evaluated in the thermomechanical model, the uncertainties in experimental datasets used for validation can also influence the evaluated mean square error; therefore, it is also useful to evaluate the confidence interval of the prediction.

2) Model Validation With Outdoor Datasets: The power degradation model (1) with $k_i = k_T$ [total degradation rate (6)] was calibrated using the monitored dataset of Gran Canaria. The dataset from Gran Canaria was selected over Negev and Zugspitze because the module in Gran Canaria has been exposed for quite a long time compared with the ones in Negev and Zugspitze, and moreover, it shows a clear degradation trend. A filter at module temperature (30–35 °C) and irradiance (800–1200 W/m^2) was used because it is the most frequent temperature that a module experiences over its lifetime in this region (see Fig. 3). The irradiance bin ensures that only clear sky conditions were considered in order to have irradiance conditions near to standard test conditions (STC) and to model a common situation for all the climates. The power was corrected to STC of irradiance. To make sure that the power degradation observed for outdoor modules is not due to soiling effects, periodic cleaning of the modules is done.

TABLE IV
EXTRACTED MODEL PARAMETERS FOR OUTDOOR MODULES

Model	A_i	n, X, θ	$E_a(eV)$
Hydrolysis (3)	4.91e7	1.90	0.74
Photo-degradation (4)	71.83	0.63	0.45
Thermo-mechanical (5)	2.04	2.24	0.43

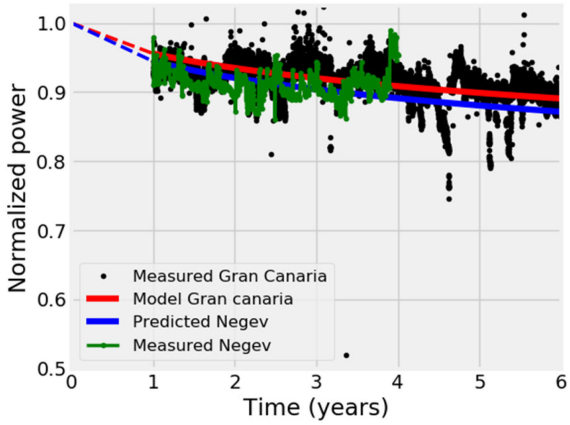

Fig. 12. Combined model (7) calibration and validation with 5-min resolution.

The extracted rate model parameters are presented in Table IV. The percentage deviation of the fitted data points was 2.34% and the derived parameters were $B = 190$ and $\mu = 0.19$ for the power function (1).

Fig. 12 shows calibration and validation results. The black dots are the measured power for Gran Canaria; the red line is the respective model fit. The blue line is the predicted power for Negev, and the measured power for Negev is in green. The dotted lines indicate normalization to the initial laboratory power values before outdoor exposure. The alpine predictions were left out to avoid too much information on the graph due to data fluctuations. The outdoor predictions show a good agreement with the measured power degradation.

D. Degradation Rates and Lifetime Prediction

Depending on the climate a module is installed in, different degradation modes might dominate over the others. Using the proposed degradation models (3)–(5) and (7) and the outdoor derived model parameters, it is possible to predict the dominating degradation precursor and the total degradation rate, as well as the failure time (8) for any location with known climatic loads.

TABLE V
PREDICTED DEGRADATION RATES USING (3)–(5) AND (7) OF THE mc-Si MODULES AND FAILURE TIME (8) IN THE THREE CLIMATIC ZONES

Location	k_h (%/year)	k_P (%/year)	k_{Tm} (%/year)	k_T (%/year)	Failure time (years)	Lower 95% CI (years)	Upper 95% CI (years)
Negev	0.169	0.216	0.225	0.74	21.4	16.7	27.1
Canaria	0.122	0.212	0.104	0.50	31.6	25.0	40.0
Zugspitze	0.043	0.103	0.129	0.30	52.8	42.7	65.0

In this paper, annual degradation rates of the mc-Si modules were predicted using input climatic loads of Zugspitze, Gran Canaria, and Negev, as shown in Table V.

High thermomechanical degradation is predicted for Zugspitze in comparison with Gran Canaria because of high module temperature variations in this climate zone. On the contrary, small degradation due to hydrolysis is predicted in Zugspitze despite the high levels of RH. This could be explained by the low average module temperatures experienced in this region, hence slowing hydrolysis processes and the absolute water vapor concentration. In all cases, high rates are predicted in Negev. This can be explained again by the higher temperatures in this zone that determines the reaction rates for other degradation processes caused by other degradation factors such as hydrolysis by humidity and photodegradation by UV dose. The predicted failure time defined as a 20% loss in power, as expected, shows more severe degradation of the maximum power output in arid climates where temperatures are higher. This further confirms the previous studies [20] that temperature could be the primary accelerator of degradation.

E. Evaluation of Uncertainties Due to Data Quality

The module power measurements were done every 5 min; such high-resolution measurements and the frequently fluctuating environmental conditions outdoors lead to unavoidable noise even after applying filters and corrections. By using a moving average of 1 h to minimize the noise in the datasets, the process of model calibration and validation was repeated. The effect of the noise to the derived model parameters as well as on failure time estimation was evaluated. Because of the high sensitivity of the models parameters, E_a, n, X, and θ, they were assumed constant, and the variations in calibration and lifetime estimations due to the noise effect are evaluated using the parameter B of the power degradation function (1).

Fig. 13 shows the calibration and validation results for hourly resolution. The deviation of the fitted data points reduced to 2.04%, and the derived model parameter reduced to $B = 182.3$

Table VI shows the MSEP and relative difference in failure time estimation with 5-min data and hourly averaged data. Although the fitting deviation improved from 2.23% to 2.04% using hourly resolution, the improvement did not considerably led to reduction in MSEP, but the effect is visible in failure time estimation with a relative difference of 4.05%. This is consistent with the observations from indoor results that the uncertainties in experimental datasets used for validation can also influence the evaluated MSEP.

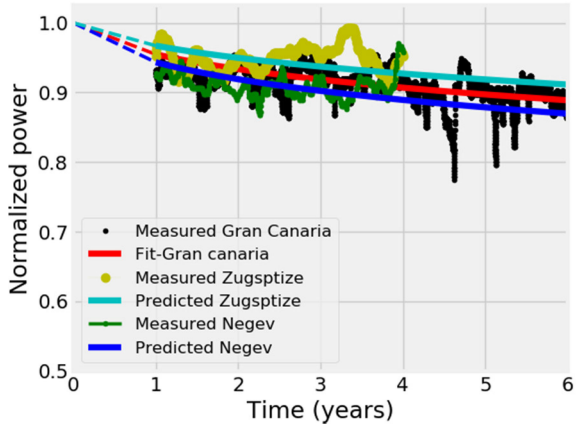

Fig. 13. Combined model (7) calibration and validation with hourly resolution.

TABLE VI
PERCENTAGE MEAN ERROR IN PREDICTION (MSEP) AND RELATIVE DIFFERENCE (REL-DIFF) OF THE ESTIMATED FAILURE TIME (t_f) FOR DIFFERENT DATA RESOLUTIONS (DATA RES)

Model	Data res	B	MSEP (%)	t_f (years)	Rel-diff
Negev	5 min	190.0	0.0230	21.4	4.05%
	Hourly	182.3	0.0240	20.5	
Zugspitze	5 min	190.0	0.0152	52.8	4.05%
	Hourly	182.3	0.0150	50.7	

V. CONCLUSION

A degradation model for quantifying the impact of combined climatic stresses on module maximum power output degradation has been introduced. Degradation rate models have been proposed and validated with indoor measurements for specific degradation precursors. A combined degradation rate model has been proposed and validated with real field datasets. The model has been applied for the evaluation of the degradation rates and the prediction of losses in the power output of monocrystalline modules installed in three climatic zones: maritime, arid, and alpine. A stronger degradation has been predicted in an arid climate, which could be explained by a higher mean module temperature, as well as high temperature variations in this zone.

In addition, a correlation of dominating degradation precursors to the operating climate has been analyzed for the three climates. Thermomechanically induced modes dominate in Zugspitze and Negev due to high temperature variations in these zones. In Gran Canaria, photodegradation dominates due to high UV values and relatively high average module temperatures experienced in this region.

The proposed power degradation model presented in this paper has been calibrated and validated using specific modules design and technology. However, the formulations are flexible and could be applied to other modules designs and technologies.

Apart from the uncertainties due to models' derived parameters and input datasets, some degradation modes might be outcomes of other degradation modes and might appear at certain stages of a module's lifetime. This makes the predictions more complex using only analytical models like the one described in this paper, hence impacting the model accuracy especially for longer time predictions. One way to solve this problem could be to apply a combination of analytical models with data-driven models or apply computer algorithms embedded with analytical models to determine the best solution for predicting outdoor service lifetime.

REFERENCES

[1] G. B. Gaines, R. E. Thomas, G. T. Noel, T. S. Shilliday, and V. E. Wood, "Development of an accelerated test design for predicting the service life of the solar array at Mead, Nebraska," Jet Propulsion Lab, Pasadena, CA, USA, Tech. Rep. DOE/JPL-954328-79/11, Jun. 1979.

[2] A. B. Subramaniyan, R. Pan, J. Kuitche, and G. TamizhMani, "Quantification of environmental effects on PV module degradation: A physics-based data-driven modeling method," *IEEE J. Photovolt.*, vol. 8, no. 5, pp. 1289–1296, Sep. 2018.

[3] S. Lindig, I. Kaaya, K. Weiß, D. Moser, and M. Topic, "Review of statistical and analytical degradation models for photovoltaic modules and systems as well as related improvements," *IEEE J. Photovolt.*, vol. 8, no. 6, pp. 1773–1786, Nov. 2018.

[4] W. Q. Meeker and L. A. Escobar, "Pitfalls of accelerated testing," *IEEE Trans. Rel.*, vol. 47, no. 2, pp. 114–118, Jun. 1998.

[5] J. Zhu, D. Montiel-Chicharro, T. R. Betts, and R. Gottschalg, "Correlation of degree of EVA crosslinking with formation and discharge of acetic acid in PV modules," in *Proc. 33rd Eur. Photovolt. Sol. Energy Conf. Exhib.*, 2017, pp. 1795–1798.

[6] M. Kempe, "Modeling of rates of moisture ingress into photovoltaic modules," *Sol. Energy Mater. Sol. Cells*, vol. 90, pp. 2720–2738, Oct. 2006.

[7] V. Sharma and S. S. Chandel, "Performance and degradation analysis for long term reliability of solar photovoltaic systems: A review," *Renew. Sustain. Energy Rev.*, vol. 27, pp. 753–767, Nov. 2013.

[8] A. Ndiaye *et al.*, "Degradations of silicon photovoltaic modules: A literature review," *Sol. Energy*, vol. 96, pp. 140–151, Oct. 2013.

[9] A. Gok *et al.*, "Predictive models of poly(ethylene-terephthalate) film degradation under multi-factor accelerated weathering exposures," *PLoS ONE*, vol. 12, no. 5, May 2017, Art. no. e0177614.

[10] J. Zhu *et al.*, "Changes of solar cell parameters during damp-heat exposure," *Prog. Photovolt. Res. Appl.*, vol. 24, no. 10, pp. 1346–1358, Oct. 2016.

[11] D. C. Jordan, T. J. Silverman, J. H. Wohlgemuth, S. R. Kurtz, and K. T. VanSant, "Photovoltaic failure and degradation modes," *Prog. Photovolt. Res. Appl.*, vol. 25, no. 4, pp. 318–326, 2017.

[12] M. L. Marín, A. Jiménez, J. López, and J. Vilaplana, "Thermal degradation of ethylene (vinyl acetate)," *J. Thermal Anal.*, vol. 47, no. 1, pp. 247–258, Jul. 1996.

[13] N. Park, W. Oh, and D. H. Kim, "Effect of Temperature and humidity on the degradation rate of multicrystalline silicon photovoltaic module," *Int. J. Photoenergy*, vol. 2013, Dec. 2013, Art. no. 925280.

[14] D. Wu, J. Zhu, T. R. Betts, and R. Gottschalg, "Degradation of interfacial adhesion strength within photovoltaic mini-modules during damp-heat exposure," *Prog. Photovolt. Res. Appl.*, vol. 22, no. 7, pp. 796–809, Jul. 2014.

[15] M. Koehl, S. Hoffmann, and S. Wiesmeier, "Evaluation of damp-heat testing of photovoltaic modules," *Prog. Photovolt. Res. Appl.*, vol. 25, no. 2, pp. 175–183, Feb. 2017.

[16] M. Koehl, M. Heck, and S. Wiesmeier, "Modelling of conditions for accelerated lifetime testing of humidity impact on PV-modules based on monitoring of climatic data," *Sol. Energy Mater. Sol. Cells*, vol. 99, pp. 282–291, Apr. 2012.

[17] L. A. Escobar and W. Q. Meeker, "A review of accelerated test models," *Statist. Sci.*, vol. 21, no. 4, pp. 552–577, Nov. 2006.

[18] D. C. Jordan, T. J. Silverman, B. Sekulic, and S. R. Kurtz, "PV degradation curves: Non-linearities and failure modes," *Prog. Photovolt. Res. Appl.*, vol. 25, no. 7, pp. 583–591, Jul. 2017.

[19] M. D. McKay, "Evaluating prediction uncertainty," Nucl. Regulatory Commission, Rockville, MD, USA, Rep. NUREG/CR-6311, 1995.

[20] E. Annigoni *et al.*, "Modeling potential-induced degradation (PID) in crystalline silicon solar cells: From accelerated-aging laboratory testing to outdoor prediction," in *Proc. 32nd Eur. Photovolt. Sol. Energy Conf. Exhib.*, 2016, pp. 1558–1563.

Authors' photographs and biographies not available at the time of publication.